Tribology International 131 (2019) 73–82

Contents lists available at ScienceDirect

Tribology International

journal homepage: www.elsevier.com/locate/triboint

Stable and unstable friction in fretting contacts

Jouko Hintikka[a,b,*], Antti Mäntylä[a], Joona Vaara[a], Tero Frondelius[a,c], Arto Lehtovaara[b]

[a] R&D and Engineering, Wärtsilä, P.O.Box 244, 65101, Vaasa, Finland
[b] Tribology and Machine Elements, Laboratory of Materials Science, Tampere University of Technology, P.O. Box 589, 33101, Tampere, Finland
[c] University of Oulu, Erkki Koiso-Kanttilan katu 1, 90014, Oulu, Finland

ARTICLE INFO

Keywords:
Fretting
Stick-slip
Friction
Wear

ABSTRACT

Designing contacts susceptible to fretting is a challenging task due to uncertainties related to friction. For example, coefficient of friction has shown to vary as a function of load cycles and so-called non-Coulomb friction can exist during individual load cycles. Concepts of stable and unstable friction are presented in this manuscript. Based on experiments, no fretting is to be expected if the utilization of friction is kept below unstable friction threshold. If contact is subjected to tangential load above this threshold, reciprocating slippage, fretting, is to be expected even if the contact was initially in stick. Experimental evidence for existence of such threshold is presented in form of friction data, slip data and fretting scars.

1. Introduction

Fretting stands for reciprocating surface sliding and wear and fatigue damage associated with it. Commonly in fretting, the slip amplitude is low, in range of few micrometers; however, it can be tens or even hundreds of micrometers. Fretting wear is characterized by occurrence of finely textured wear debris, which tends to entrap inside the contact. Fretting fatigue is considered especially harmful due to potentially catastrophic component failures and by the fact that fretting fatigue failure initiates inside the contact and thus is difficult to be observed. Fretting induced surface degradation accelerates fatigue crack initiation, making evaluation of fretting fatigue loads difficult. A more comprehensive description of fretting and contacts is available in these Refs [1–3].

Engine designer wants to squish out most of the available engine performance leading to high utilization of material strength. This narrows acceptable margin of error, both in the loads and the material strength sides. Design against fatigue is made difficult by the presence of highly loaded contacts due to additional uncertainties related to fretting induced friction and surface degradation. It is well known that fretting can impair components fatigue endurance [1,2]; hence, it may be desirable to avoid fretting altogether [4,5]. Before this can be achieved, the designer needs to know how much of the available friction can be safely utilized, though this is made difficult by the fact that non-idealities, such as non-Coulomb friction and friction instabilities exists [6], as demonstrated in this introduction.

The running condition of fretting contact can be fully stuck, in partial slip (PS) or in gross sliding (GS), depending on the contact geometry, coefficient of friction (*COF*) used materials and imposed forces and displacements [3,7]. Partial slip may occur if friction force is less than the product of *COF* and normal force, and in the case of Hertzian sphere-on-plane contact this will lead condition, where the contacts outer annulus slips while central region remains stuck [3]. In gross sliding, all of the contacting surface experience sliding. There is also mixed slip fretting regime, where the running condition changes during fretting cycling, for example due to changing *COF* [8].

Concentrated contacts or incomplete contacts, such as the Hertzian point contact, are highly usable in fretting research, but are somewhat limited in achievable contact size. Regardless, it has been demonstrated that considerable size effects exists both in fretting fatigue [9] and in fretting wear [10,11], which rises concern to the engineers mind when implementing fretting research findings to machine design because component interfaces tend to be orders of magnitude larger than the fretting contacts used in literature. Complete contacts, such as annular flat-on-flat type contacts [12,13] can alleviate some of the limitations of incomplete contacts. It is also possible to achieve full stick conditions with complete contacts, which is hard to achieve using incomplete contacts.

COF is very important variable in fretting contacts [3]. For example, *COF* has strong effect on the running condition of the contact, amount of slip and on the tangential traction contributing directly on overall cyclic stresses. Fretting induced friction has been reported extensively covering steels and aeronautical alloys; however, it is common to only report the values of *COF* assuming ideal Amontons/Coulomb friction

* Corresponding author. R&D and Engineering, Wärtsilä, P.O.Box 244, 65101, Vaasa, Finland.
E-mail address: jouko.hintikka@wartsila.com (J. Hintikka).

https://doi.org/10.1016/j.triboint.2018.10.014
Received 10 July 2018; Received in revised form 16 September 2018; Accepted 11 October 2018
Available online 22 October 2018

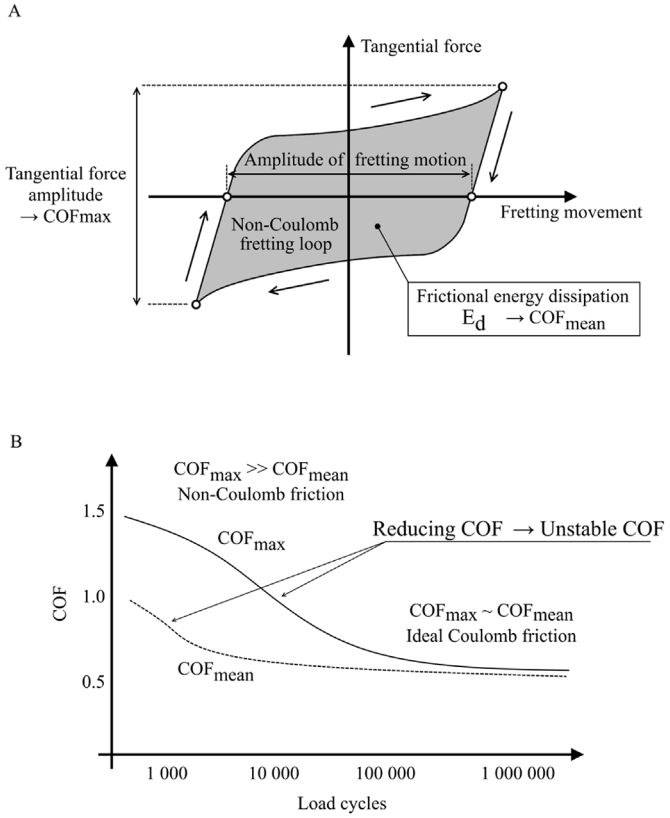

Fig. 1. Schematic illustrations of (A) Non-Coulomb fretting loop and (B) development of *COF* s as a function of load cycles.

($COF = Q/P$) [14,15]. However, there exist non-idealities in fretting induced friction which are often ignored in literature. So-called non-Coulomb friction phenomenon was investigated in detail by Mulvihill et al. [16] and by Hintikka et al. [17]. In ideal conditions, friction remains at constant value during sliding, and individual points in sliding contact will produce parallelogram slip-tangential-traction -graphs. However, under Non-Coulomb friction, the tangential force increases during the gross sliding phase within one load cycle and leads to 'hook'-shaped fretting loops, shown schematically in Fig. 1. It has been shown that non-Coulomb friction is caused by adhesive wear damage leading to material transfer and formation of tangentially interlocked protrusions and depressions, which causes mechanical interlocking and inclined sliding inside the interface [16,17]. Non-Coulomb friction may occur also in incomplete contacts due to macroscopic interlocking, when relatively hard fretting pad digs a trench to the specimen surface due to fretting wear or plastic deformation [18–20].

Uniform *COF* does not capture the variable nature of fretting induced tangential force very well under Non-Coulomb friction conditions. One approach to get a better understanding of overall frictional behaviour is to use two *COFs*. Average *COF* (COF_{mean}) can be calculated form the measured fretting loops conveniently once frictional energy dissipation E_d and fretting motion amplitude are extracted [13,18–20], or by calculating average tangential force weighed by corresponding fretting motion from the gross sliding part of the loop [21]. The maximum *COF* during fretting load cycle can be calculated simply from the tangential force amplitude [12,13] (Fig. 1A). It is possible to take into a count variable friction conditions, as demonstrated in Refs. [22–24], but this introduces an extra level of complexity to the analysis of fretting prone components.

Engineering surfaces have certain amount of roughness depending on the used manufacturing methods. Contact between two such surfaces is characterized by the presence of multiple asperity tip contacts, where the true contact area is by far the smaller than the nominal contact area [25,26]. In the contact of rough surfaces, tangential load will introduce compliance in the tangential direction composing of solid body elastic deformation [3] and deformation and slippage in individual asperity tip contacts [27]. Modeling of fretting wear under constant normal load partial slip conditions has shown that it leads to gradual wearing down of slipping region and that the normal and tangential loads are carried entirely by the remaining tick region, both in the case of Herzian line [28] and point [29] contacts. Interestingly, in both cases, the shape and size of the final stick region corresponds to the initial partial slip stick region. However, it has been shown that the stresses become severe at the edge of the final stick region and that the presence of plasticity can lead additional plasticity-induced-wear [30]. Regardless, the wearing down of slip region, and the concentration of tangential and normal tractions should lead to reduced stiffness in tangential direction, not just in the case of single Herzian contact but also in the case of rough surfaced contacts as well, assuming that individual asperity tip contacts behave somewhat similar to Hertzian point contacts.

Fretting fatigue limit and -life may be evaluated using different fatigue criteria [31,32]. Often such methods can be implemented in FE-analysis [33,34] greatly increasing their usability in industrial applications. Regardless, all of the methods require realistic estimates of the *COF* because it can have huge effect on the resulting stresses and strains. Quenched and tempered steel (QT) is a good material for a component under high fatigue load, i.e. in combustion engines, QT may be used in crankshafts and connecting rods. Fretting induced frictional behaviour of QT-QT contact is characterized by initial friction peak, where the measured *COF* gets very high values, in range of 1.4–1.6, during the first few hundred load cycles, and after peaking it reduces gradually to much lower value and stabilizes to about 0.7 (Fig. 1B) [12,13]. Initial high *COF* conditions are also accompanied by non-Coulomb friction [13,17]. This friction behaviour, where the *COF* shows dramatic reduction in its value is labelled here as unstable friction. The question is: how much of the available friction can be utilized without encountering such unstable friction? This is crucial information for an engineer.

This study aims to find out how much of the available friction can be utilized before friction starts to show unstable behaviour, observed previously in gross sliding fretting experiments, and when fretting damage starts to occur. Fretting experiments are run in stick and partial slip conditions. Hence, only a fraction of the available friction was utilized in these experiments. This is full length manuscript of previously published abstract [35].

2. Experimental

2.1. Fretting apparatus

Fretting test were done using so-called annular flat-on-flat test rig. The device is presented here only briefly and more comprehensive description can be found from Ref. [13]. In the test set-up, fretting contact occurs between two identical and axisymmetric specimens with annular contact surfaces. The specimens are attached to fixed and detachable specimen holders respectively. Hydraulic cylinder provides the normal load via the fixed specimen holder, while reciprocating fretting movement is provided by an electric shaker via lever arm rotating the detachable specimen holder. The normal load P, torque T and rotation θ are measured with 5000 Hz frequency, while the fretting loading frequency was 40 Hz. The rotation is measured with eddy current probe from a distance of 100 mm from the symmetry axis. Frictional torque is measured with strain gauges in full Wheatstone bridge configuration and normal load with commercial s-beam load cell. Schematic illustration of the contact conditions is shown in Fig. 2.

2.2. Specimens

The inner and outer radiuses (r_i and r_o) of the used annular contact

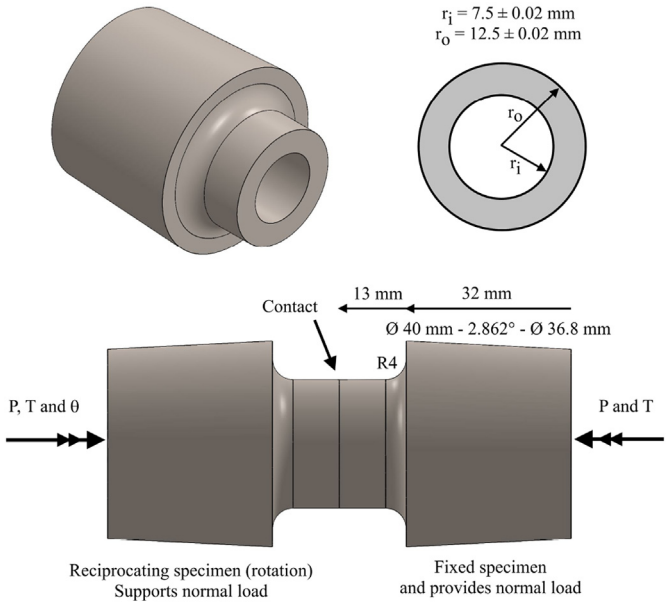

Fig. 2. Annular flat-on-flat contact.

were 7.5 mm and 12.5 mm respectively. The specimens were turned into shape from 45 mm diameter steel rod (EN 10083-1-34CrNiMo6 + QT). This material has yield strength of 1056 MPa and ultimate strength of 1150 MPa. The contact surface was fine ground so that the scratching marks were circular, hence parallel to the fretting movement. Specimens were cleaned thoroughly using ultrasonic cleaner, first in acetone and then in ethanol. 3D-profilometer (Wyco NT1100) was used to measure the surface roughness of all specimens. Arithmetic mean surface roughness Sa was in range of [0.14–0.27] μm and peak valley height St in range of [1.8–4.9] μm.

2.3. Measurements

Fretting experiments were run at 30 MPa normal pressure and at different *TR* -levels so that only portion of the available friction was utilized. *TR* stands for traction ratio and is fully defined in section 3.4, though it is analogous to tangential force to normal force ratio in linear motion. Average normal pressures and measured rotation amplitudes (P and θ_{am}), and maximum TR that resulted (TRM), are listed in Table 1. Although the apparatus was run under rotation amplitude control, it was possible to run these experiments without any modifications to the test rig control, because specimen elastic deformation under torque lead to large enough rotation to be accurately measured and controlled, even though the interface remains stuck. The peak value for COF_{max} was previously measured to be about 1.38 in gross sliding, while its stabilized steady state value was about 0.77. On the other hand, the steady state value for COF_{mean} was about 0.68. In this study, the target *TR* values were in range of 0.3–1.0 covering values above and below stabilized COF_{max} and COF_{mean}, so that test points are located above and below both gross sliding steady state *COFs*. Total of 20 experiments were conducted in this study.

Table 1
Measurement matrix.

TRM [−]	0.28	0.35	0.36	0.43	0.46	0.51	0.56
P [N]	9330	9487	9367	9381	9350	9213	9371
θ_{am} [mRad]	0.299	0.398	0.400	0.503	0.502	0.601	0.627
TRM [−]	0.56	0.68	0.74	0.75	0.93	0.94	0.96
P [N]	9317	9333	9357	9201	9340	9369	9194
θ_{am} [mRad]	0.632	0.798	0.844	0.844	1.049	1.056	1.054

Experiments were run following the procedure already explained in detail in Ref. [13]. In short, the specimens were attached to the apparatus, their relative parallelism was corrected using pressure sensitive film (Fuji Prescale), and the target surface normal pressure was applied. Then the rotation amplitude was increased linearly from zero to the target level in the first 10 s (400 load cycles), after which it was kept at a constant for the remainder of the experiment. The test duration was $3.0*10^6$ load cycles for each test. Measurements were run in ambient laboratory atmosphere at 24 °C–28 °C and at a relative humidity of 8%–24%.

2.4. Data analysis

All measured signals were fully recorded and stored, though full duration data was later sampled to reduce file size and analysis time. One-second-long samples were extracted with exponentially increasing time steps providing lots of samples from the early parts of the experiments, when *COF* changes the most, while latter parts of the experiment were analyzed with less data samples. Each sample contains 40 fretting load cycles, though only five first complete fretting load cycles were extracted and average fretting loop was calculated reducing signal noise. These average fretting loops were then used in subsequent data analysis.

3. Analytical

This section describes the mechanics of fretting annular contact which was used in the experiments. It is demonstrated that this kind of contact can be in stick, partial slip and in gross sliding. However, the average values of slip amplitude and tangential traction divided by normal traction can be obtained using the same equations that have been used previously to analyze gross sliding conditions [13,17].

3.1. Finite element model

3.1.1. Model description

Normal traction distribution of the used annular contact was solved using FE in 2D (Abaqus), utilizing axisymmetry (Fig. 3A). Used element type was linear quadrilateral with reduced integration (CGAX4R). The element size was 50*100 μm in the contact, giving total of 100 elements over the contact and the necessary mesh fidelity was verified by using 10*20 μm elements (500 elements over the contact). The entire tubular section had this element size. The element size was allowed to grow up to 800 μm towards the conical part of the specimen. The interface was modeled using Lagrange friction formulation. Specimens conical surfaces were coupled rigidly to the reference points RP1 and RP2, which were then used to load the contact with normal load (step-1) and rotation (subsequent steps). In the test rig, specimens are fixed to the specimen holders using these conical surfaces. The normal load step was modeled using only one increment; however, all rotation steps were modeled using at least 100 increments per half cycle. In all simulations the average normal pressure was 30 MPa similar to experiments. The FE-model is shown schematically in Fig. 3A.

The total number of elements and -variables (degrees of freedom plus Lagrange multiplier variables) were 41051 and 125272 for the 50 μm model and 826036 and 2488827 for the 10 μm model, respectively.

3.1.2. Normal- and tangential tractions

The shape of normal- and tangential traction distributions were simulated using $COF = 1.0$. The contact was load with rotation amplitude large enough to cause gross sliding (1.2 mRad). Total of 200 loading increments were used so that the tangential traction could be extracted for stick, different stages of partial slip and gross sliding. The normal traction distribution could be extracted simply after the first normal

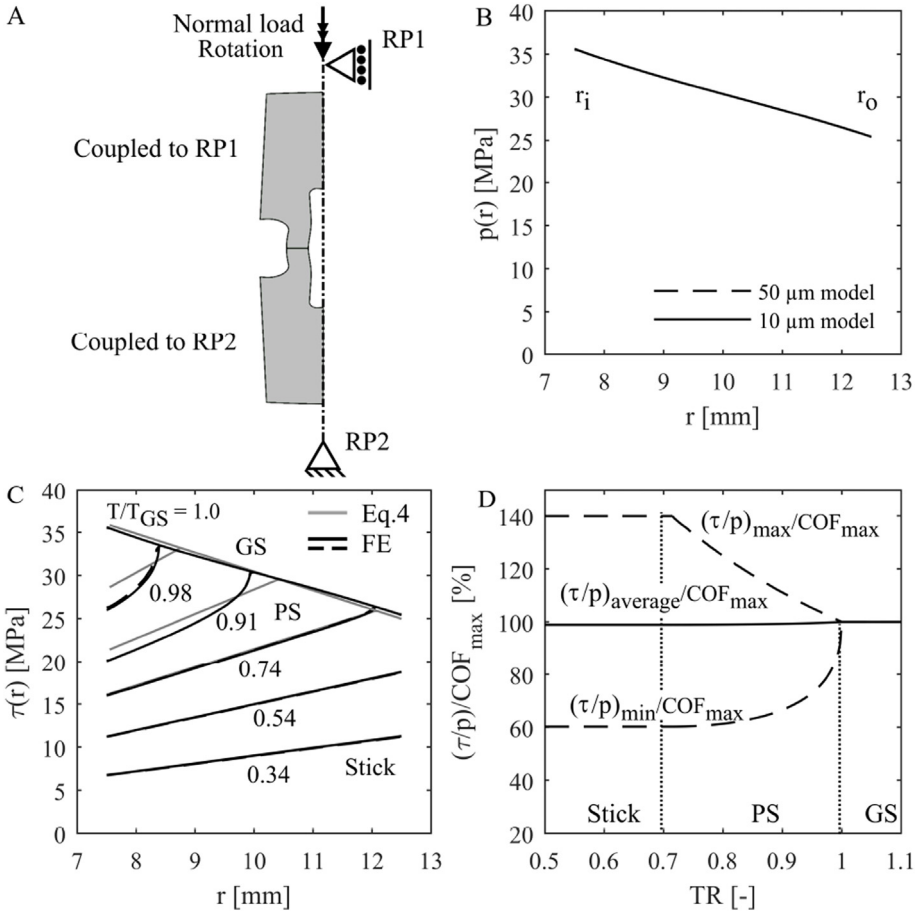

Fig. 3. (A) Axisymmetric FE model, (B) Normal and (C) tangential tractions in annular contact and deviation of $(\tau/p)/COF_{max}$ -ratio in the contact when the contact transitions from stick to gross sliding (p = 30 MPa, COF = 1.0).

load step.

3.1.3. Partial slip fretting cycles

Partial slip conditions were simulated using different COF s (0.50, 0.68, 0.77 and 1.0) and different rotation amplitudes. The specimens were first fretted at two extreme positions (half cycle) followed by removal of rotation boundary condition, leading to loading condition where imposed torque becomes zero. The remaining rotation was extracted from the resulting zero torque condition. The torque amplitude and zero-torque-based rotation amplitudes were then extracted. Also, the slip distribution was analyzed.

This zero-torque-based rotation value was used to analyze the amount of slippage in experiments. Hence, slippage was analyzed using same approach in FE-simulations than what was used to analyze the experiments, and then simulation was compared against experimental result.

3.2. Simple analytical solution for tangential traction

Annular contact, under reciprocating rotation load, can be in gross sliding if the motion is large enough and in stick if the motion or torque is low enough; however there exist also partial slip region in between. The shape of tangential traction distribution depends on the running condition. In gross sliding tangential traction is simply the product of COF and normal traction distribution $p(r)$ as shown in Eq. (1). In stick, the tangential traction is equal to shear stress in hollow circular cross-section under torque load, and is proportional to the radius r, torsional constant I_p of the cross-section (Eq. (2)) and torque T as shown in Eq. (3). Assuming rigid bodies, tangential traction in partial slip may be estimated according to Eq. (4), which is Eq. (3) limited by Eq. (1) in magnitude. Only circumferential component of tangential traction is considered here because the radial component is insignificant in comparison.

$$\tau_{GS}(r) = COF*p(r) \quad (1)$$

$$I_p = \pi/2*(r_o^4 - r_i^4) \quad (2)$$

$$\tau_{Stick}(r) = r*T/I_p \quad (3)$$

$$\tau(r) = min(\tau_{Stick}(r), \tau_{GS}(r)) \quad (4)$$

3.3. Normal and tangential traction distributions

It was found out that the normal pressure is the highest at the inner edge of the contact and that it reduces nearly linearly towards the outer edge of the contact (Fig. 3B), and that the deviation from average normal pressure is about 18% at maximum. Previously only the tubular part of the specimen was modeled and the deviation was reported to be about 5% [13]. However, in COF calculations a constant normal pressure can be assumed because the error is less than 1% even if $p(r)$ has ± 18% deviation.

Partial slip conditions were also modeled using Matlab, based on Eq. (4), where it was assumed that $p(r)$ reduces linearly from inner to outer specimen radius with approximately ± 18% deviation from nominal normal pressure according to Fig. 3B.

The shapes of tangential traction distributions are illustrated in Fig. 3C for different torque levels so that all running conditions are covered. The ratio T/T_{GS} represents the fraction between torque at

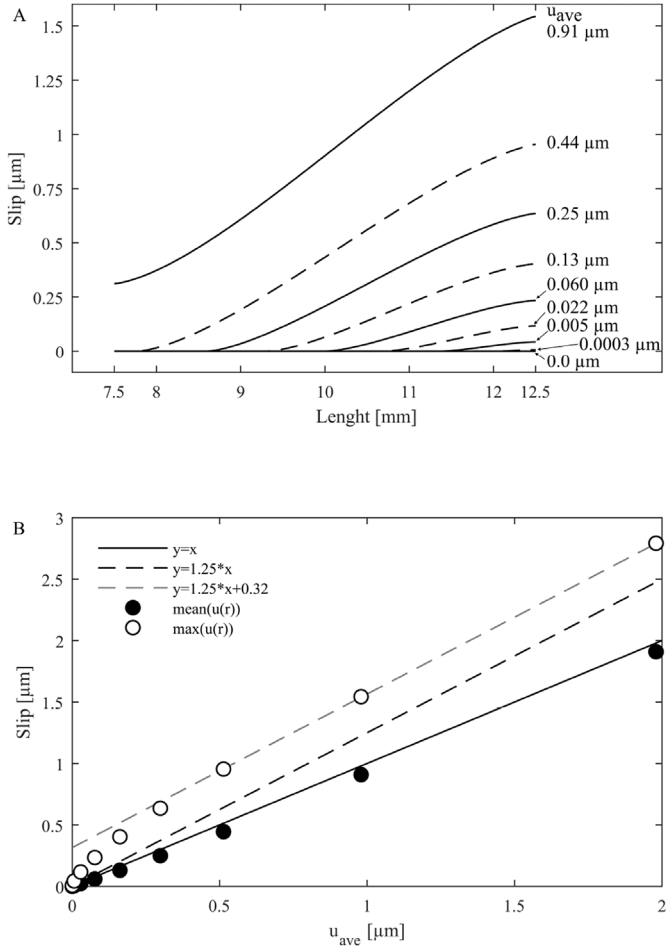

Fig. 4. (A) Slip distribution u(r) and (B) u_{ave} and maximum slip from FE-simulation with.$COF = 1.0$

current load level (T) and in gross sliding (T_{GS}). The black and gray curves were solved using FE-modeling and Eq. (4), respectively. In stick and in gross sliding FE-modeling and Eq. (4) produce nearly identical results for $\tau(r)$; however, deviation exist in partial slip. Basically, the FE solution has slightly larger slipping area due to the stresses and deformation in the close proximity of stick-slip-boundary for a given T/T_{GS} -level, alleviating in the stick region by a small amount.

In Fig. 3B&C, solid and black lines represent the result obtained using 10 μm and 50 μm models, respectively. In the case of normal pressure, no difference can be seen between the two models. In the case of tangential traction the FE-models produce nearly identical results, the only differences being at the proximity of stick/slip boundary. Largest difference in Fig. 3C come from small variation in solution incrementation. It can be concluded that the mesh is refined enough even with the 50 μm model.

3.4. *COF and Traction ratio TR*

In gross sliding, *COF* can be calculated using different approaches [13]. The simplest one is based on the torque amplitude and it represents the contacts maximum resistance against fretting motion (COF_{max}, Eq. (6)). Slip $u(r)$ and tangential traction produce frictional energy dissipation E_d (Fig. 1A), corresponding to the area inside fretting loop. Assuming rigid bodies, and that $\tau(r) = COF{*}p(r)$ and that $u(r) = \theta{*}r$, *COF* can be calculated from the E_d and θ amplitude according to Eq. (7) (COF_{mean}). This COF_{mean} represents the mean *COF* during one fretting cycle and it gives better predictions of true *COF* than COF_{max}, especially under non-Coulomb friction conditions. The rotation amplitude in Eq. (7) can be obtained conveniently from fretting loops when $T = 0.0Nm$.

$$T_0 = 2\pi \int_{r_i}^{r_o} r^2{*}p(r)\, dr \tag{5}$$

$$COF_{max} = T_a/T_0 \tag{6}$$

$$COF_{mean} = E_d/[4{*}\theta_a{*}T_0] \tag{7}$$

It is important to realize that COF_{max} and COF_{mean} represent *COF* values during single fretting cycle; however, both *COF* s can vary as a function of load cycles. Therefore, both COF_{max} and COF_{mean} can have their own minimum, average and maximum values [13,17]. These equations hold true only in gross sliding conditions and *COF* remains unknown in stick and in partial slip conditions. In fact, solutions for *COF* in partial slip conditions are only available for certain types of contacts, such as Hertzian sphere-on-plane contact [36,37]. In this study, measurements were made in conditions where friction was only partially utilized, and hence *COF* remains unknown. The ratio between tangential and normal tractions is used instead, obtained by integrating τ/p -ratio over the entire contact and by dividing by the contact area A according to Eq. (8).

$$(\tau/p)_{average} = (2\pi/A){*}\int_{r_i}^{r_o} r{*}(\tau/p)\, dr \tag{8}$$

The Eq. (8) was solved using linearized version of $p(r)$ and Eq. (4) solution for $\tau(r)$. The result was compared against COF_{max} in Fig. 3D showing that difference between Eq. (6) and Eq. (8) is only about 1% in stick condition and the difference reduced gradually to zero when contact goes in to gross sliding. Hence it may be concluded that COF_{max} is a good estimate for $(\tau/p)_{average}$. Of course average traction ratio does not represent *COF* in stick or in partial slip conditions, therefore Eq. (6) is renamed here as traction ratio *TR* according to Eq. (9):

$$TR \equiv COF_{max} \tag{9}$$

TR is analogous to friction force to normal load -ratio in linear motion. It is important to realize that tangential traction has certain kind of distribution depending on the *COF* and imposed loads as demonstrated in Fig. 3C. Though *TR* is nearly equal to $(\tau/p)_{average}$, the τ/p -ratio has also a distribution of values. For example, in stick conditions τ/p -ratio is up to 40% greater than *TR*, at the contacts outer edge (r_o). Similarly, the inner edge is subjected to lower τ/p -ratio than what is obtained by using *TR*. These values gradually become equal to *TR* when the running condition transition from partial slip to gross sliding as illustrated in Fig. 3D. Regardless; *TR* is a good estimate for $(\tau/p)_{average}$ -ratio in all running conditions.

3.5. *Slip distribution and zero-torque-based slip amplitude*

Slip amplitude can be estimated conveniently in gross sliding conditions from the zero-torque-based rotation amplitude $\theta_{T=0Nm}$. Using this method the displacements caused by specimen and apparatus elastic deformations are automatically removed. Average slip amplitude is obtained by using Eq. (10), where r_a is the average radius (10 mm).

$$u_{ave} = r_a{*}\theta_{T=0Nm} \tag{10}$$

This method does not take into account the slip distribution in partial slip conditions, which is shown Fig. 4A. In partial slip running condition the slip amplitude is very small and increases nearly linearly from the stick slip boundary towards specimen outer edge. However, the average slip calculated from r_i to r_o, including zero slip in sticking region, is very close the Eq. (10) prediction (Fig. 4B). Regardless, slip distribution exists both in partial slip and in gross sliding.

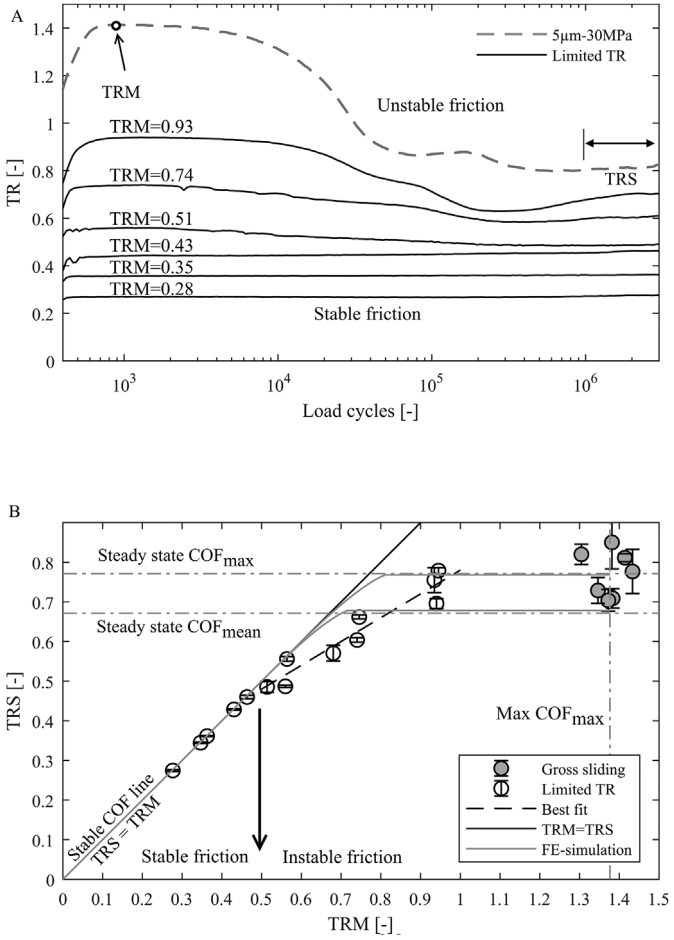

Fig. 5. (A) *TR* -curves and (B) *TRM* − *TRS* chart.

4. Results

4.1. TR-curves

Fig. 5A shows the measured *TR* -curves as a function of load cycles. At high *TR* -levels the curves showed similar kind of unstable frictional behaviour than what has been observed in previous gross sliding fretting experiments. Initially, *TR* was high and then it gradually reduced and stabilized to a lower value. Unstable friction was more pronounced the higher the *TR* -level was. On the other hand, when the target *TR* -level was reduced, friction behaved in increasingly stable manner, and fully stable friction was observed at the lowest *TR* -levels.

The maximum and stabilized values of *TR* were extracted from the data, labelled here as *TRM* and *TRS*, respectively. *TRM* is simply the maximum of measured *TR*, and *TRS* was calculated as average of measured TR considering last two million load cycles (see Fig. 5A). It is possible to evaluate the stability of friction by comparing the values of *TRM* and *TRS*. Basically, stable friction prevails if $TRM = TRS$, and unstable friction prevails if $TRM > TRS$. Furthermore, the greater the difference between *TRM* and *TRS* the greater the instability. Fig. 5B shows *TRM* − *TRS* graph including all test points run in this study and gross sliding test points from previous study [13] with 30 MPa normal pressure for reference. The error bar represents the minimum and maximum values.

Fig. 5B illustrates that at low *TR* levels the friction remains stable and that unstable friction prevails at high *TR* levels. Least square linear fit to test points showing unstable friction ($TRM > TRS$) intersects stable friction line ($TRM = TRS$) when *TR* is about 0.45. Though, looking at the data in Fig. 5, a threshold value of about 0.5 can be extracted. Taking into a count that in stick conditions the local maximum of τ/p -ratio is 40% larger than *TR* at specimens outer edge, it follows that the threshold value is actually locally in range of 0.6–0.7 which is very close to previously measured steady state COF_{mean} of 0.68.

The simulated *TRM* − *TRS* curves are included in the Fig. 5B, representing ideal transition from initial high *COF* to lower steady state *COF*, taking into account different sliding conditions and specimen compliance similar to experiment conditions. Measured points fall slightly below curves obtained from FE-simulations, based on assumptions of ideal geometry and ideal Amontons/Coulomb friction, which indicates that the magnitude of measured instability cannot be explained entirely by transition from stick to partial slip, due to reducing *COF*.

Though, unstable friction begins at *TR* of about 0.5, the measured *TRS* increases when *TRM* is increased, but the slope is less than 1. This indicates that fretting contact has a capacity to carry higher friction than the stable friction threshold level allows.

4.2. Fretting loops

Examples of fretting loops are shown in Fig. 6. At lowest TR-levels Fig. 6A&B the fretting loops are narrow, producing very little frictional energy dissipation. Also, the fretting loops remain largely unchanged through out the experiment.

At TR-levels greater than 0.5 the fretting loops start to show more hysteresis and also the shape of the fretting loops changes to wider shape as the experiment progresses, leading to increasing frictional energy dissipation.

4.3. Slip

Rotation amplitude was extracted from the fretting loops from the locations when torque was equal to zero, as an average value from forward and reverse movement (Fig. 1A). Sliding amplitude was calculated as rotation amplitude times the average specimen radius of 10 mm. Of course, in stick, sliding cannot occur and in partial slip conditions there exist sliding and sticking regions, and slip has distribution of values in the sliding regime. Also in gross sliding, true slip increases towards outer edge of the contact where it is 25% larger than the calculated average value. Regardless, the calculated u_{ave} represents the average slip in the entire annular contact.

Fig. 7A shows examples how u_{ave} develops as a function of load cycles with different target *TR* levels. At low *TR* -levels u_{ave} remains at a constant value and close to zero; however, at high *TR* -levels u_{ave} tends to increase as a function of load cycles, which occurs simultaneously when measured *TR* reduces (Figs. 5A).

Averages of calculated u_{ave} over entire measurement duration as a function of *TRM* are shown in Fig. 7B, where the error bar represents the minimum and maximum values. At low *TR* -levels, measured u_{ave} was close to zero. However once *TRM* was greater than about 0.5, u_{ave} started to increase in a linear fashion. Obviously, u_{ave} is independent of *TR* in gross sliding. The dashed line represents least square linear fit to data points showing unstable friction, from which a threshold value of 0.41 can be extracted for the *TR* -threshold. Again, the corresponding maximum *TR*, at the outer edge of the specimen, is in range of 0.6–0.7.

Solid black lines with dots in Fig. 7B represent FE-model results for u_{ave} -TR-dependence. In these simulations, transition from partial-slip to gross-sliding occurred in between the last two black dots (~0.5 µm). Basically the measured u_{ave} was much larger than what can be obtained from the simulations, especially once TR-level exceeded value of about 0.5. It is not possible to explain the amount of measured u_{ave} with a constant *COF* and ideal contact conditions.

Both the u_{ave} and *TR* change during the experiment when *TR* exceed the threshold value of about 0.5 and unstable friction prevails. Measured *TR* versus u_{ave} was approximately linear as illustrated in Fig. 5C, where gradually reducing *TR* leads to gradually increasing u_{ave}.

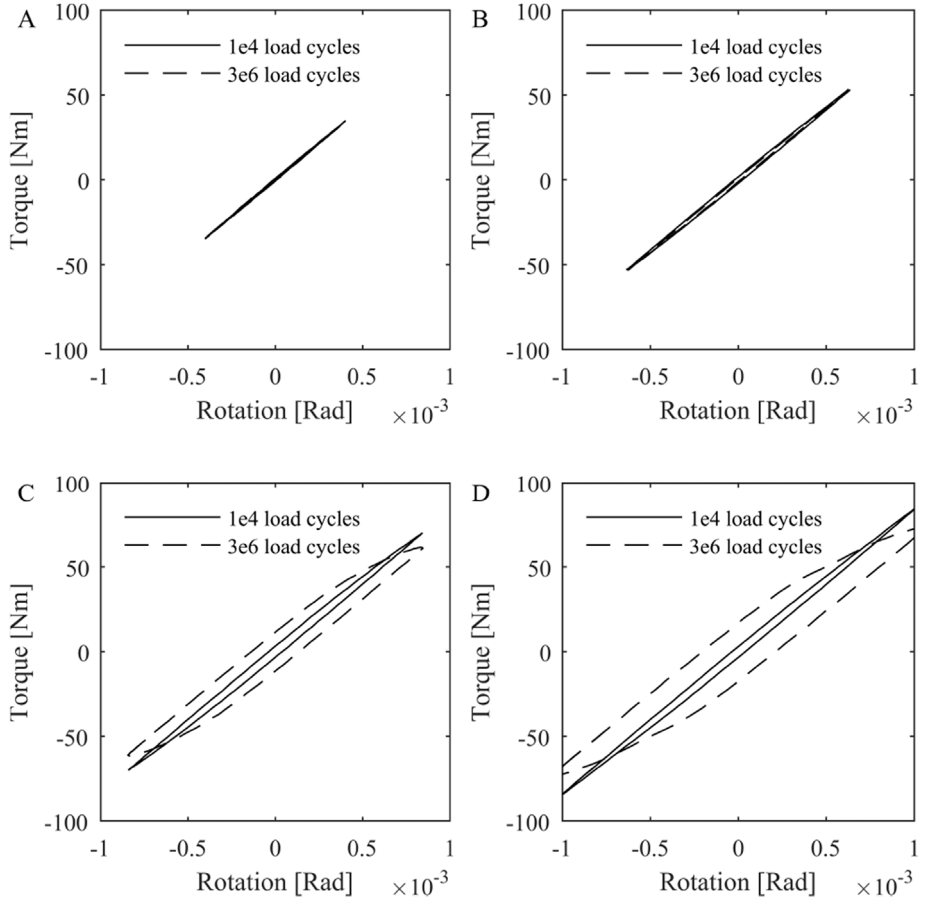

Fig. 6. Example fretting loops from the beginning and from the end of the experiment at different *TR* -levels (A) $TRM = 0.35$, (B) $TRM = 0.51$, (C) $TRM = 0.74$ and (D) $TRM = 0.93$.

The experiment was run under rotation amplitude control and the control signal is composed of slip and specimen elastic deformation under torque load, therefore reducing friction lead to increasing u_{ave} because friction controls the amount of rotational compliance in the specimens. Note that the slope of the u_{ave} vs. TR-curves represents the specimens torque stiffness.

4.4. Fretting scars

Compilation of fretting scars is shown in Fig. 8. All fretting scars showed only limited amount of fretting wear damage in comparison to previous gross sliding fretting scars [13]. At low *TR* -levels, fretting scars showed barely visible wear damage, though minute amounts of brown oxidation could be observed from all specimens.

The fretting wear damage was barely visible to *TR* -levels up to 0.56; however, there is a clear trend of increasing fretting wear damage as a function of *TR* after this load level. Based on the fretting scars, a threshold *TR* for fretting wear damage is in the range of 0.5–0.6. This threshold corresponds closely to the ones extracted from the *TR* -data and slip-data. Overall, the wear damage was limited to individual spots, which most likely represents true asperity tip contacts. These spots could be found in multiple locations throughout the contact.

Sometimes the damage was more concentrated at the inner edge and sometimes at the outer edge, which may be attributed to the actual combination of specimens' surface roughness's and manufacturing accuracy. None of the fretting scars showed conclusive evidence of existence of partial slip, where sliding is limited to the outer annulus while central annulus remains intact. It would have been interesting to try to quantify the wear volume as a function of TR, for example using 3D-profilometry. However, such investigation was not done this time but it remains as a potential future study.

5. Discussion

Observed frictional behaviour, slip, and fretting wear damage at low *TR* -levels have shown that there exists a threshold- *TR*, below which the frictional behaviour remains stable, slip is limited to very low values, and fretting scars shown barely visible damage. However, exceeding this threshold *TR* value of about 0.5, leads to increasing *COF* instability, increasing slip amplitude and increasing fretting wear damage. It is likely that this threshold corresponds to transition from stick to partial slip/gross sliding. Under such conditions, τ/p -ratio has local maximum at the edge of the contact with value of about 0.7. Most importantly, this threshold value is significantly lower than the maximum of COF_{max}; however, this value is very close to previously measured steady state COF_{mean}. This means, that even though the contact could momentarily carry higher friction loads than what $COF = 0.7$ allows, such load level would ultimately lead to fretting conditions.

In previous gross sliding fretting studies, it was demonstrated that non-Coulomb friction originates from mechanical tangential fretting scar interactions, caused by formation and shearing of fretting induced cold-weld junctions and that the gradual reduction in the COF_{max} occurs when the tangential fretting scar interactions reduce in magnitude possibly due to wearing down of interlocked protrusion and depressions or by wear debris accumulation. None of the specimens showed evidence of severe adhesive wear damage, even though slippage had occurred. However, the slippage was nearly zero during the first thousands of load cycles. It may be that the magnitude of slip during the first thousands of load cycles plays a critical role on the severity of adhesive wear damage and formation of non-Coulomb friction conditions.

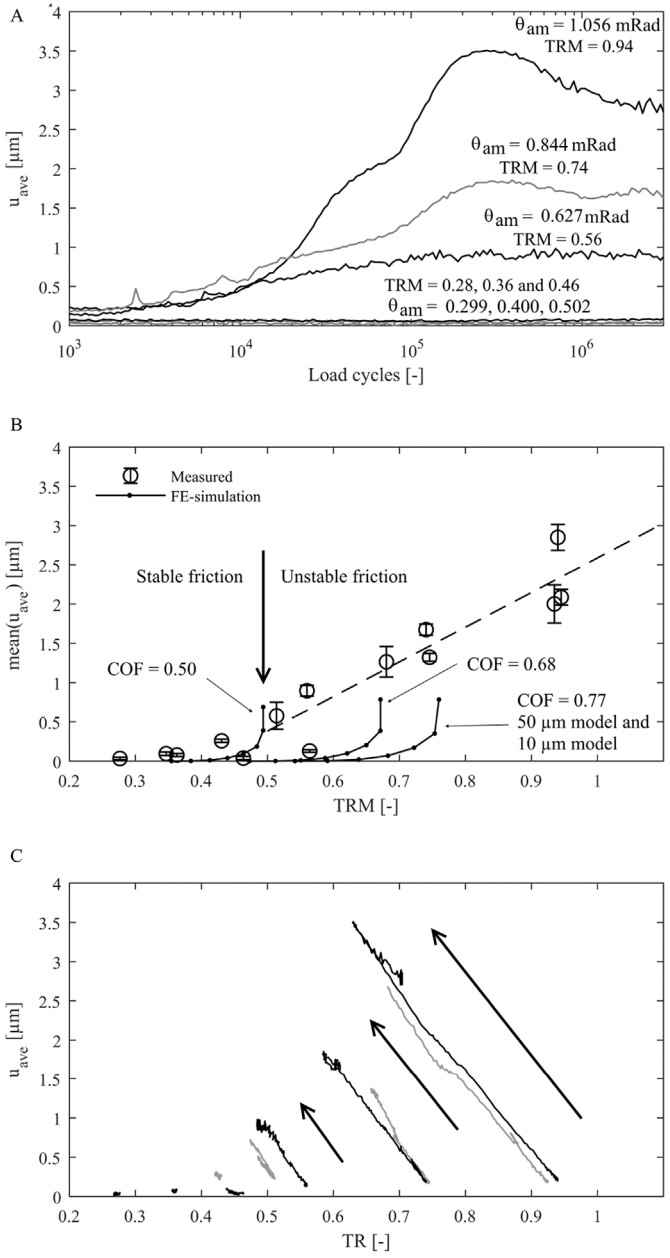

Fig. 7. (A) Examples of measured u_{ave} at various load levels, (B) *TRM* vs mean (u_{ave}) in experiments and FE-simulations and (C) u_{ave} dependence on *TR* during various experiments where black and gray lines represent repeated measurements.

Regardless, it is possible that shearing and breaking down of asperity tip junctions starts to occur once threshold to unstable fiction is exceeded, and that the entire phenomenon of unstable friction is caused by fretting wear that follows. Alternative explanation for the unstable friction could be that the threshold value represents the load at asperity tip contact level, where fatigue limit of asperity tip junctions has been exceeded. The threshold value may be interpreted as shear strength or shear fatigue limit of fretting interface.

In partial slip conditions, the annular contact should wear from the outer edge of the contact. Assuming that wear debris is readily ejected, it follows that the normal pressure should reduce at the sliding annulus and sticking inner annulus should experience increasing contact pressure. It might even be possible that partial slip contact goes back to fully stuck conditions once wear has removed and ejected enough material from the sliding outer annulus. This kind of contact should have lower

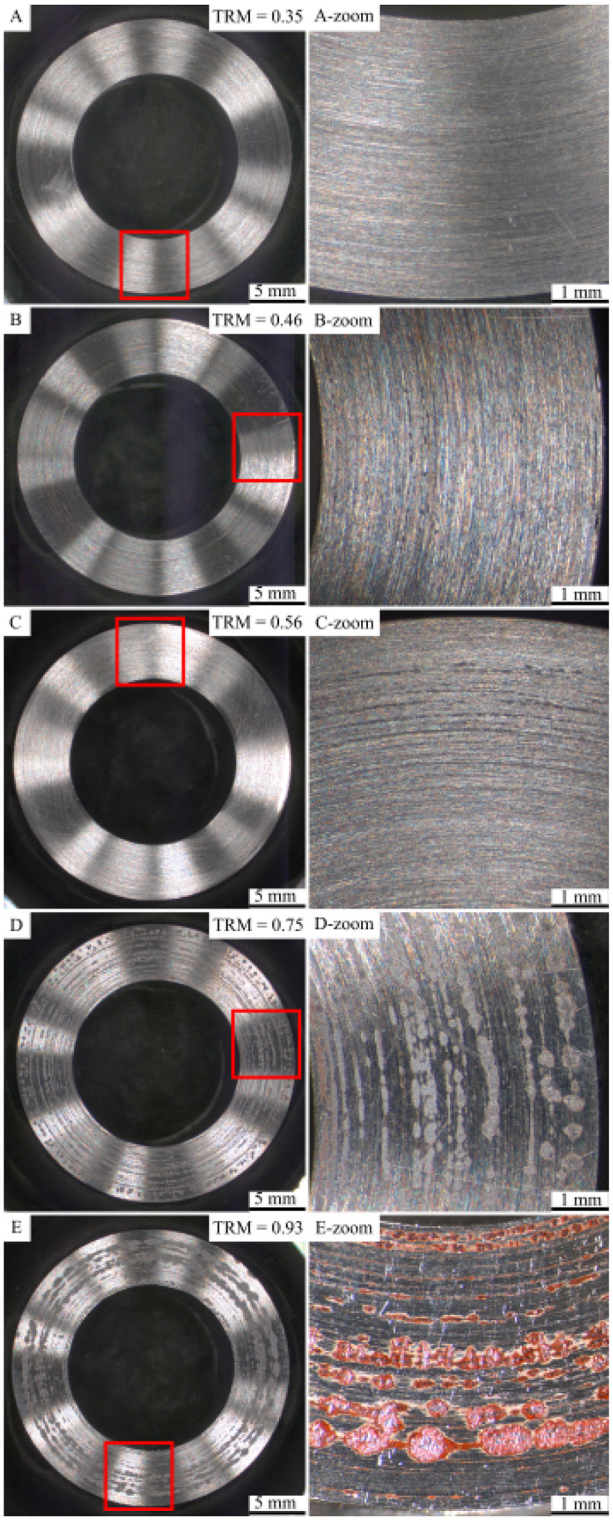

Fig. 8. Measured fretting scars. *TR* -level increases from up to bottom.

torque stiffness in comparison to initial conditions due to reduced nominal contact area, which could explain why *TR* reduces gradually as a function of load cycles in the unstable *COF* regime (Fig. 5A). However, this not valid explanation based on observations on how the slip amplitude develops (Fig. 7A) because it should lead to more narrow fretting loops with less hysteresis and lower slip amplitudes. The fretting loops become wider instead producing more frictional dissipation and greater slippage. Therefore, partial slip and wearing down of

sliding annulus cannot explain observed unstable friction.

One possible explanation for the measured unstable friction is partial slip that occurs at the level of individual asperity tip contacts. The specimens used in this study had finely ground surfaces, therefore contact was between roughs surfaces rather than ideally flat ones. As described in the introduction, the contact between rough surfaces has certain amount of tangential compliance originating from the slip and deformation at asperity tip level. The wearing down of individual asperity tip contacts might then lead to gradually reducing tangential stiffness. However, the wearing down of slipping regions at asperity tip level should lead towards elastic conditions; whereas measurements showed increasing slip and increasing frictional dissipation. Furthermore, it has been observed in other studies that fretting wear debris tends to get entrapped inside the contact instead, leading to drastically different conditions. Fretting wear and resulting accumulating wear debris may contribute on the friction instability. A thin layer of entrapped oxidized wear debris may accommodate fretting motion more readily than contact of intact steel surfaces.

A threshold value level for usable friction utilization is convenient for engineers designing fretting prone components. Based on these results dry QT-QT fretting contact may be subjected to maximum τ/p -ratio of about 0.7, while average value for entire contact was about 0.5. It may even be reasonable to use the average value instead of the maximum as it is more conservative. Maximum value was obtained using assumptions of ideal contact geometry and ideal COF. It is possible to exceed these τ/p -ratio; however, it will lead to unstable friction, sliding and fretting wear damage. Basically, high non-Coulomb friction measured in the gross sliding conditions cannot be utilized in component design without risk of fretting damage.

6. Conclusions

Fretting experiments were only a fraction of the available friction was used in order to study friction instability phenomenon previously measured in gross sliding conditions using dry quenched and tempered steel fretting contact. The goal was to find out how much of the available friction can be safely utilized without risk of fretting. Following conclusions were drawn:

- Friction instability exist in gross sliding, where friction is high during the early parts of fretting experiment, gradually reducing to much lower steady state values. Similar friction instability exists in loading regime where only a fraction of the available friction is used, though there is τ/p -threshold where stable friction transitions to unstable friction. This threshold has average value over entire fretting contact of about 0.5 and corresponding local maximum at the specimen outer edge is about 0.7.
- The previously mentioned threshold value of 0.7 corresponds closely to gross sliding steady state coefficient of friction (COF_{mean}); however, it is significantly lower than the peak value for COF_{max}, which is about 1.4.
- Measured sliding was nearly zero and stable when load levels were low; however, it increased gradually when the previously mentioned threshold load was exceed.
- Fretting wear damage was insignificant at load levels below the threshold load level and increased gradually once the threshold was exceeded. Modest excess did not cause severe fretting damage.
- Fretting contact has capacity to carry higher friction loads, than dictated by the stable/unstable friction threshold; however, increasing amounts of slippage and fretting wear will follow. This indicates that the threshold TR represents also fretting damage threshold.

Acknowledgements

This study was conducted as part of the MaNuMiES (Dnro 3361/31/2015) and WIMMA (Dnro 1566/31/2015) -research projects. The authors are grateful for the financial support provided by Business Finland Oy (former Tekes), Wärtsilä Finland Oy, Agco Power Oy and Global Boiler Works Oy.

References

[1] Waterhouse R. Fretting corrosion. Oxford: Pergamon press; 1972. ISBN 0 08 16902 3, ISBN ISBN 0 08 16902 3.
[2] Hills D. Mechanics of fretting fatigue. Kluwer Academic Publishers; 1994. ISBN 0-7923-2866-3, ISBN ISBN 0-7923-2866-3 https://doi.org/10.1016/0043-1648(94)90173-2.
[3] Johnson K. Contact mechanics. Cambridge: Cambridge University Press; 1985. ISBN ISBN 0 08 16902 3.
[4] Mäntylä A, Göös J, Leppänen A, Frondelius T. Large bore engine connecting rod fretting analysis. Rakenteiden Mekaniikka 2017;50(3):239–43. https://doi.org/10.23998/rm.64914.
[5] Niva J. Frettingsäröjen etenemisen tutkiminen murtumismekaniikan avulla. Rakenteiden Mekaniikka 2017;50(3):186–90. https://doi.org/10.23998/rm.64935.
[6] Hintikka J, Juoksukangas J, Lehtovaara A, Frondelius T, Mäntylä A. Non-idealities in fretting contacts. Rakenteiden Mekaniikka 2017;50(3):171–4. https://doi.org/10.23998/rm.64886.
[7] Vincent L, Berthier Y, Dubourg M, Godet M. Mechanics and materials in fretting. Wear 1992;153(1):135–48. ISSN 0043-1648 https://doi.org/10.1016/0043-1648(92)90266-B.
[8] Zhou Z, Vincent L. Mixed fretting regime. Wear 1995;181–183:531–6. ISSN 0043-1648 https://doi.org/10.1016/0043-1648(95)90168-X. 10th International Conference on Wear of Materials.
[9] Nowell D, Dini D, Hills D. Recent developments in the understanding of fretting fatigue. Eng Fract Mech 2006;73(2):207–22. ISSN 0013-7944 https://doi.org/10.1016/j.engfracmech.2005.01.013. [advanced Fracture Mechanincs for Life Safety Assessments].
[10] R M, S F. Contact size effect on fretting wear behaviour: application to an AISI 52100/AISI 52100 interface. Lubric Sci 2009;21(3):83–102.
[11] Warmuth A, Pearson S, Shipway P, Sun W. The effect of contact geometry on fretting wear rates and mechanisms for a high strength steel. Wear 2013;301(1):491–500. ISSN 0043-1648 https://doi.org/10.1016/j.wear.2013.01.018. wear of Materials 2013.
[12] Leidich E, Maiwald A, Vidner J. A proposal for a fretting wear criterion for coated systems with complete contact based on accumulated friction energy density. Wear 2013;297(1):903–10. ISSN 0043-1648 https://doi.org/10.1016/j.wear.2012.11.006.
[13] Hintikka J, Lehtovaara A, Mäntylä A. Fretting-induced friction and wear in large flat-on-flat contact with quenched and tempered steel. Tribol Int 2015;92:191–202. ISSN 0301-679X https://doi.org/10.1016/j.triboint.2015.06.008.
[14] Tobi AM, Ding J, Bandak G, Leen S, Shipway P. A study on the interaction between fretting wear and cyclic plasticity for Ti–6Al–4V. Wear 2009;267(1):270–82. ISSN 0043-1648 https://doi.org/10.1016/j.wear.2008.12.039. 17th International Conference on Wear of Materials.
[15] Naidu NR, Raman SGS. Effect of contact pressure on fretting fatigue behaviour of Al–Mg–Si alloy AA6061. Int J Fatig 2005;27(3):283–91. ISSN 0142-1123 https://doi.org/10.1016/j.ijfatigue.2004.07.001.
[16] Mulvihill D, Kartal M, Olver A, Nowell D, Hills D. Investigation of non-Coulomb friction behaviour in reciprocating sliding. Wear 2011;271(5):802–16. ISSN 0043-1648 https://doi.org/10.1016/j.wear.2011.03.014.
[17] Hintikka J, Lehtovaara A, Mäntylä A. Normal displacements in non-Coulomb friction conditions during fretting. Tribol Int 2016;94:633–9. ISSN 0301-679X https://doi.org/10.1016/j.triboint.2015.10.029.
[18] Rybiak R, Fouvry S, Bonnet B. Fretting wear of stainless steels under variable temperature conditions: introduction of a 'composite' wear law. Wear 2010;268(3):413–23. ISSN 0043-1648 https://doi.org/10.1016/j.wear.2009.08.029.
[19] Fouvry S, Duó P, Perruchaut P. A quantitative approach of Ti–6Al–4V fretting damage: friction, wear and crack nucleation. Wear 2004;257(9):916–29. ISSN 0043-1648 https://doi.org/10.1016/j.wear.2004.05.011.
[20] Lavella M, Botto D. Fretting wear characterization by point contact of nickel superalloy interfaces. Wear 2011;271(9):1543–51. ISSN 0043-1648 https://doi.org/10.1016/j.wear.2011.01.064. 18th International Conference on Wear of Materials.
[21] Hintikka J, Lehtovaara A, Mäntylä A. Non-Coulomb friction in gross sliding fretting conditions with aluminium bronze against quenched and tempered steel. Tribol Int 2014;79(151 – 161). ISSN 0301-679X https://doi.org/10.1016/j.triboint.2014.06.004.
[22] Cheikh M, Quilici S, Cailletaud G. Presentation of KI-COF, a phenomenological model of variable friction in fretting contact. Wear 2007;262(7):914–24. ISSN 0043-1648 https://doi.org/10.1016/j.wear.2006.10.001.
[23] Naboulsi S, Nicholas T. Limitations of the Coulomb friction assumption in fretting fatigue analysis. Int J Solid Struct 2003;40(23):6497–512. ISSN 0020-7683 https://doi.org/10.1016/S0020-7683(03)00401-3.
[24] Yue T, Wahab M. Finite element analysis of fretting wear under variable coefficient of friction and different contact regimes. Tribol Int 2017;107:274–82https://doi.org/10.1016/j.triboint.2016.11.044.
[25] Greenwood J, Williamson J. Contact of nominally flat surfaces. ProcRoySocLond 1966;295(1442):300–19. https://doi.org/10.1098/rspa.1966.0242.
[26] Pereira K, Yue T, Wahab M. Multiscale analysis of the effect of roughness on fretting

wear. Tribol Int 2017;110:222–31https://doi.org/10.1016/j.triboint.2017.02.024.
[27] Argatov I, Butcher E. On the Iwan models for lap-type bolted joints. Int J Non Lin Mech 2011;46(2):347–56. https://doi.org/10.1016/j.ijnonlinmec.2010.09.018.
[28] Hills D, Sackfield A, Paynter R. Simulation of fretting wear in halfplane geometries: Part 1–the solution for long term wear. J Tribol 2009;131. 031401–031401–4 https://doi.org/10.1115/1.3118785.
[29] Argatov I, Chai Y. Limiting shape of profiles in fretting wear. Tribol Int 2018;125:95–9https://doi.org/10.1016/j.triboint.2018.04.026.
[30] Lehtovaara A, Lönnqvist C. Modelling and analysis of fretting wear in rough point contacts in partial slip conditions. Proc IME J J Eng Tribol 2011;225(10):986–98. https://doi.org/10.1177/1350650111417215.
[31] Bhatti N, Wahab M. Fretting fatigue crack nucleation: a review. Tribol Int 2018;121:121–38https://doi.org/10.1016/j.triboint.2018.01.029.
[32] Gandiolle C, Garcin S, Fouvry S. A non-collinear fretting-fatigue experiment to compare multiaxial fatigue criteria: critical shear plane strategy is better than invariant formulations. Tribol Int 2017;108:57–68. ISSN 0301-679X https://doi.org/10.1016/j.triboint.2016.09.011. proceedings of The 8th International Symposium on Fretting Fatigue.
[33] Araújo J, Susmel L, Pires M, Castro F. A multiaxial stress-based critical distance methodology to estimate fretting fatigue life. Tribol Int 2017;108:2–6.https://doi.org/10.1016/j.triboint.2016.07.028. proceedings of The 8th International Symposium on Fretting Fatigue.
[34] Bhatti N, Wahab M. Fretting fatigue damage nucleation under out of phase loading using a continuum damage model for non-proportional loading. Tribol Int 2018;121:204–13https://doi.org/10.1016/j.triboint.2018.01.038.
[35] Hintikka J, Lehtovaara A, Frondelius T, Mäntylä A. Tangential traction instability in fretting contact below fully developed friction load. Rakenteiden Mekaniikka 2017;50(3):175–8. https://doi.org/10.23998/rm.65105.
[36] Mindlin R. Compliance of elastic bodies in contact. Jnl. Appl. Mech 1949;16(1):259–68.
[37] Fouvry S, Kapsa P, Vincent L. Analysis of sliding behaviour for fretting loadings: determination of transition criteria. Wear 1995;185(1):35–46. ISSN 0043-1648 https://doi.org/10.1016/0043-1648(94)06582-9.